

SUPPORTING INFORMATION:
Overlapping hydration shells in salt solutions
causing non-monotonic Soret coefficients with
varying concentration

Shilpa Mohanakumar, Hartmut Kriegs
Wim Briels and Simone Wiegand

October 18, 2022

Contents

S1 IR-Thermal diffusion Forced Rayleigh scattering set-up	S2
S2 Refractive index contrast measurements	S4
S3 Concentration dependence of S_T, D_T and D	S5
S4 Temperature dependence of S_T, D_T and D	S8

S1 IR-Thermal diffusion Forced Rayleigh scattering set-up

A detailed description of the thermal diffusion forced Rayleigh scattering technique can be found in the literature [1, 2, 3, 4, 5, 6]. We used the infrared thermal diffusion forced Rayleigh scattering (IR-TDFRS) setup [7], which is optimal for aqueous solutions. The main difference is that no dye is needed to convert the light energy into heat energy in aqueous solutions, due to the absorption of water at the wavelength of the infrared laser beam ($\lambda_w=980$ nm).

Summarizing what is explained in more detail in the above given references, the infrared laser beam is split into two beams that interfere in the sample cell, creating an intensity grating. The intensity grating is absorbed by the fluid and as a consequence, a temperature gradient builds up, which in turn causes a concentration grating by the effect of thermal diffusion. Both temperature and concentration gratings contribute to a combined refractive index grating which is read out by the Bragg diffraction of an He-Ne laser ($\lambda_w=633$ nm). The typical fringe spacing of the grating is $20\mu\text{m}$ and the amplitude of the temperature grating will be in the order of $100\mu\text{K}$ [7]. The total heterodyne scattering intensity $\zeta_{\text{het}}(t)$ assuming an ideal excitation with a step function is given by

$$\begin{aligned} \zeta_{\text{het}}(t) = & 1 - \exp\left(-\frac{t}{\tau_{\text{th}}}\right) \\ & - A(\tau - \tau_{\text{th}})^{-1} \left\{ \tau \left[1 - \exp\left(-\frac{t}{\tau}\right) \right] - \tau_{\text{th}} \left[1 - \exp\left(-\frac{t}{\tau_{\text{th}}}\right) \right] \right\} \end{aligned} \quad (\text{S1})$$

with the steady state amplitude A

$$A = \left(\frac{\partial n}{\partial c}\right)_{p,T} \left(\frac{\partial n}{\partial T}\right)_{p,c}^{-1} S_{\text{T}} c (1 - c) \quad (\text{S2})$$

where c is the mass concentration, τ_{th} the heat diffusion time, $(\partial n/\partial c)_{p,T}$ and $(\partial n/\partial T)_{p,c}$ are refractive index contrast factors in respect to mass concentration at constant pressure and temperature, and in respect to temperature at constant pressure and mass concentration, respectively. The Soret coefficient $S_{\text{T}} = D_{\text{T}}/D$ can be expressed as ratio of the thermal diffusion coefficient, D_{T} , and the collective diffusion coefficient, D . Whereas $D = 1/(q^2\tau)$ can be calculated from the diffusion time, τ , in Eq. S1 using q the magnitude of the grating vector which is given by

$$q = \frac{4\pi}{\lambda_w} \sin\frac{\theta}{2} \quad (\text{S3})$$

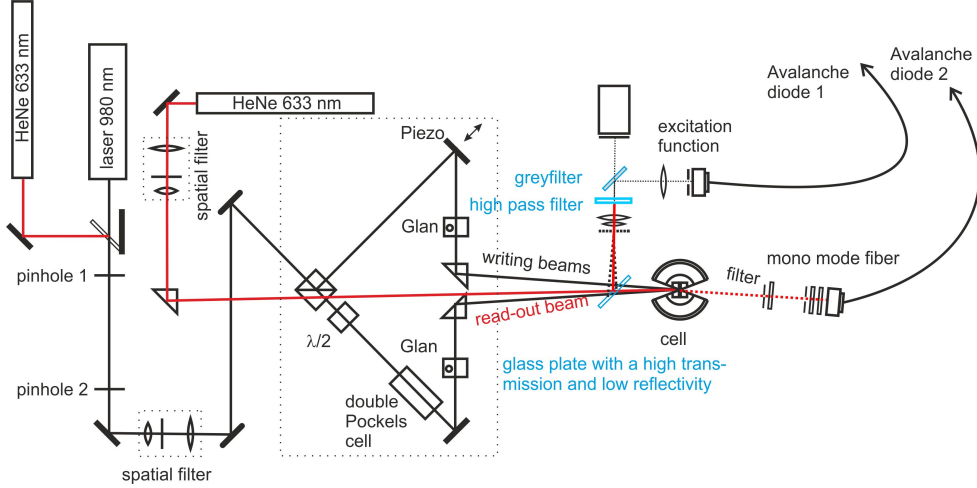


Figure S1: Sketch of the infrared TDFRS setup.

where θ is the angle between the two writing beams at the wavelength λ_w . The transport coefficients are determined by fitting Eq. S1 to the measured heterodyne signal and deconvoluting the excitation function [8, 9].

A sketch of the IR-TDFRS setup is shown in Fig. S1. We simultaneously record the excitation function and diffracted signal (through the cell), so any external disturbance (thermal or mechanical) will affect both recorded signals in the same way. This has been achieved by replacing the original flip mirrors [7] in front of the cell and the camera, by a glass plate with a high transmission and a low reflectivity and by a grey filter, respectively. Using a grey filter in front of the camera avoids ghost images on the camera due to internal reflections within the glass. For the phase synchronization of the excitation function we use a line grating, with the same period as the optical grating in its image plane. This line grating is mounted on a motorized translational stage. This can be moved perpendicular to the optical axis, so that the phase of the excitation function can be determined and adjusted. Using this additional grating reduces the noise in the determination of the phase.

S2 Refractive index contrast measurements

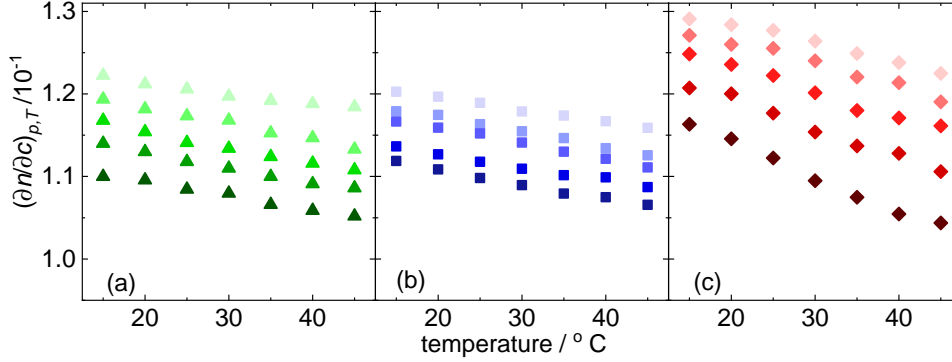


Figure S2: Contrast factor calculated from the refractive index measurements $(\partial n / \partial c)_{p,T}$ for (a) KI, (b) NaI and (c) LiI are plotted against temperature. Concentration follows the order 0.5, 1, 2, 3 and 4 mol/kg from top to bottom with highest concentration corresponding to darkest of symbols.

In order to calculate the Soret coefficient S_T from the intensity of the diffracted read-out beam, it is necessary to know the dependence of the refractive index on concentration. This was measured with an Abbe refractometer (Anton Paar Abbemat MW) at a wavelength of 632.8 nm. Fig.S2 shows the derivative of $n(c, T)$ with respect to concentration determined by linear fitting of the experimental refractive index values. $(\partial n / \partial c)_{p,T}$ decreases with increase in temperature. Measurements of the refractive index were conducted for 7 concentrations.

The dependence of the refractive index on temperature, $(\partial n / \partial T)_{p,c}$, is also necessary for the calculation of the Soret coefficient. This was measured interferometrically [10]. For the calculation of S_T from the IR-TDFRS measurements, the contrast factors were interpolated from these measurement series for temperatures and concentrations at which the TDFRS experiment had been performed. In the measured concentration and temperature range, $(\partial n / \partial T)_{p,c}$ is negative for all salts. The absolute value of $(\partial n / \partial T)_{p,c}$ increases with increasing salt concentration.

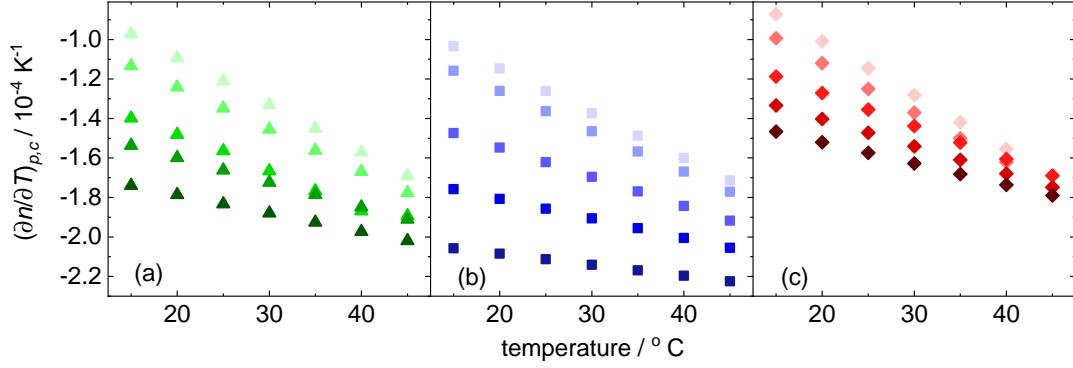


Figure S3: Results of the interferometrically measured contrast factors $(\partial n/\partial T)_{p,c}$ for (a) KI, (b) NaI and (c) LiI at different concentrations. Concentration follows the order 0.5, 1, 2, 3 and 4 mol/kg from top to bottom with highest concentration corresponding to darkest of symbols.

S3 Concentration dependence of S_T, D_T and D

As it can be seen in Fig. S4 and Fig. S5, both KI and LiI show minimum with concentration for S_T and D_T . D shows a monotonous increase with concentration for both salts. Thus behavior of these coefficients is very similar to that of NaI discussed in the main manuscript. LiI for concentrations $c > 0.75$ mol/kg shows thermophilic behavior for all temperatures. Where as KI shows thermophilic behavior at very low concentrations, $c < 2$ mol/kg at $T=15^\circ\text{C}$.

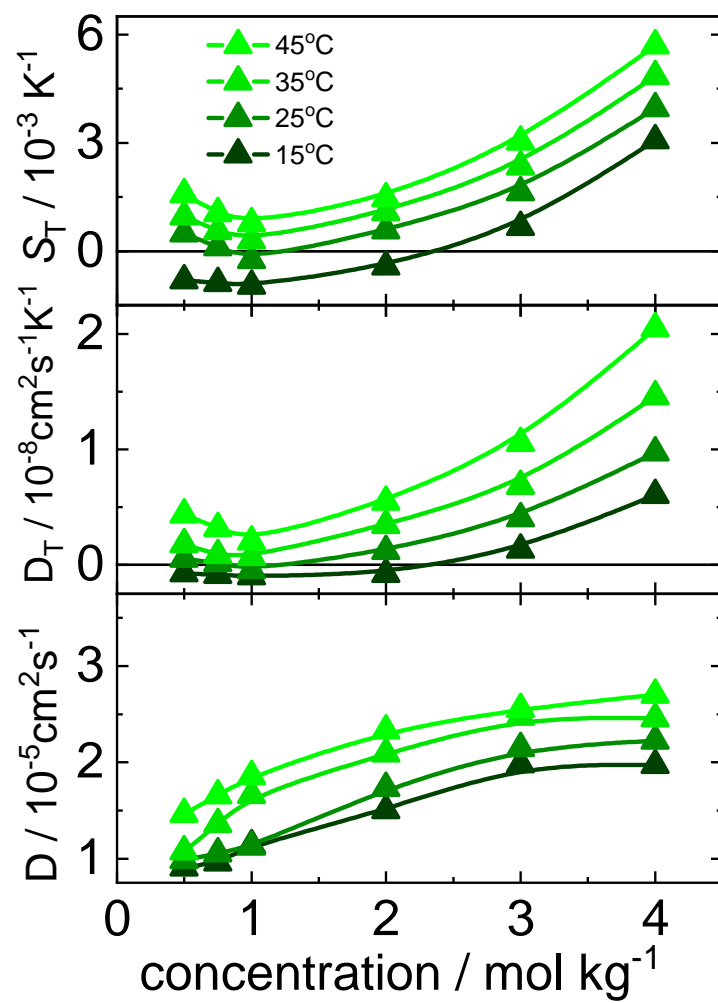


Figure S4: Concentration dependence of S_T , D_T and D of KI at four different temperatures. In each panel temperatures are 15, 25, 35 and 45 °C in the order with the darkest symbol corresponding to lowest temperature as shown in inset.

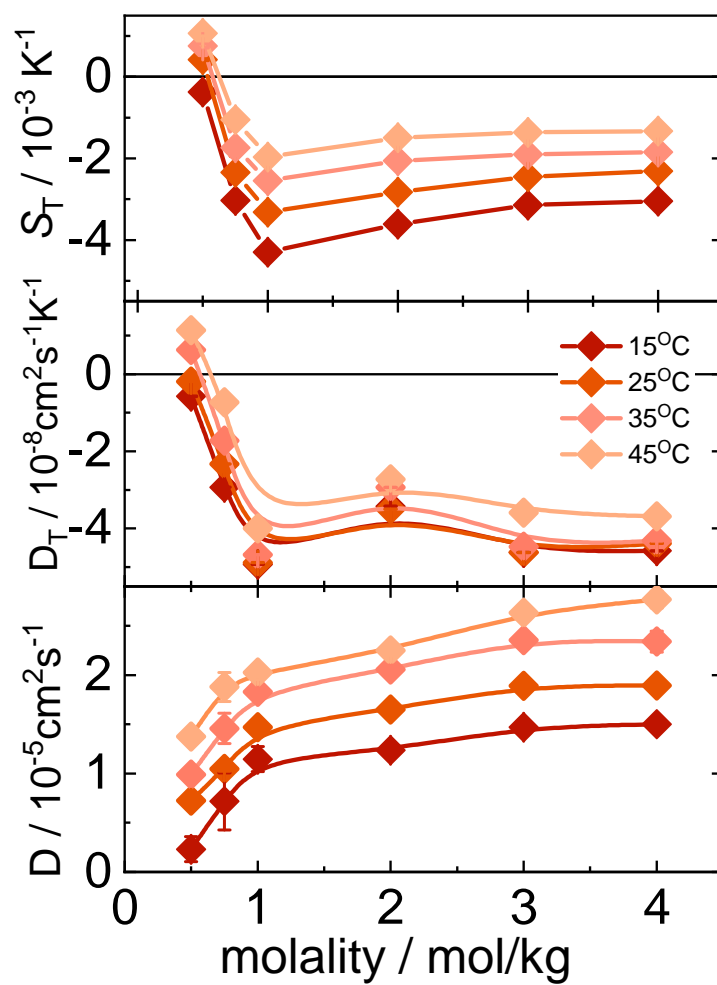


Figure S5: Concentration dependence of S_T , D_T and D of LiI at four different temperatures. In each panel temperatures are 15, 25, 35 and 45 °C in the order with the darkest symbol corresponding to lowest temperature as shown in inset.

S4 Temperature dependence of S_T , D_T and D

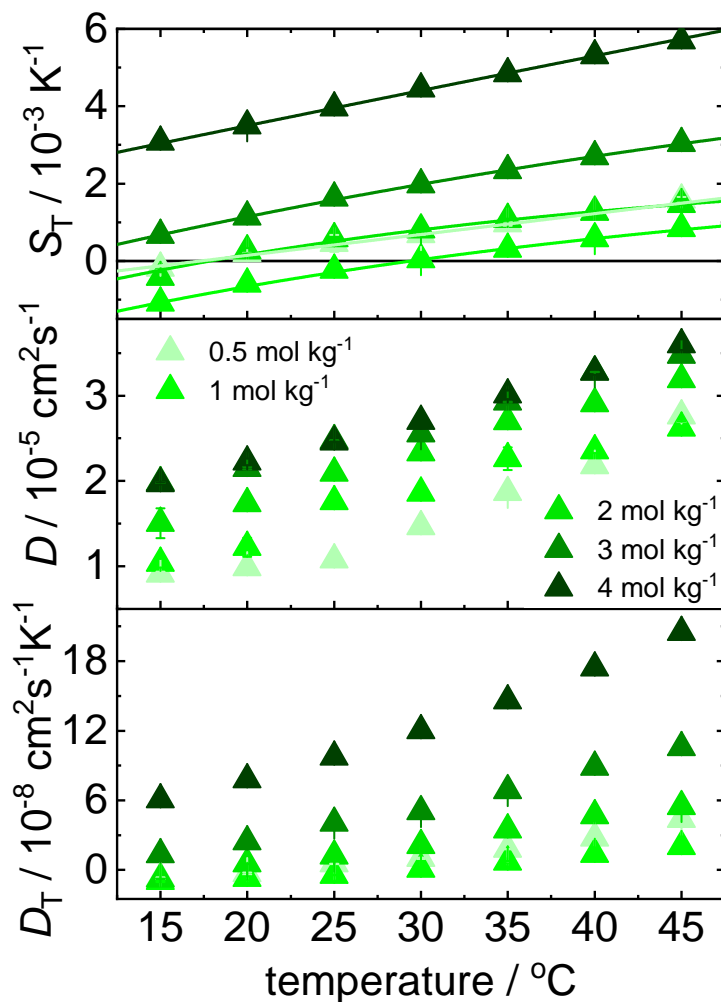


Figure S6: Temperature dependence of S_T , D_T and D of KI at different concentrations as shown in inset. The darkest symbol corresponds to the highest concentration 4 mol/kg followed by lower concentrations of 3, 2, 1 and 0.5 mol/kg (faded symbol).

Temperature dependence of S_T , D_T and D for KI, NaI and LiI is shown in Fig.S6, Fig.S7 and Fig.S8, respectively. S_T , D_T and D of all the systems increases with temperature at all concentrations measured.

Table S1: The table enlists the fitting parameters obtained for KI using Eq.2 in the main manuscript for all the concentrations studied

m / mol/kg	$S_T^\infty / 10^{-3} K^{-1}$	T^* / K	T^0 / K
0.5	2.40 ± 0.03	22.45 ± 0.21	22.7 ± 3.8
1	3.54 ± 0.08	29.45 ± 0.06	59.4 ± 6.8
2	2.61 ± 0.04	17.88 ± 1.04	32.9 ± 9.1
3	7.23 ± 0.09	8.40 ± 0.49	67.5 ± 10.1
4	8.54 ± 0.06	17.45 ± 2.33	69.4 ± 7.8

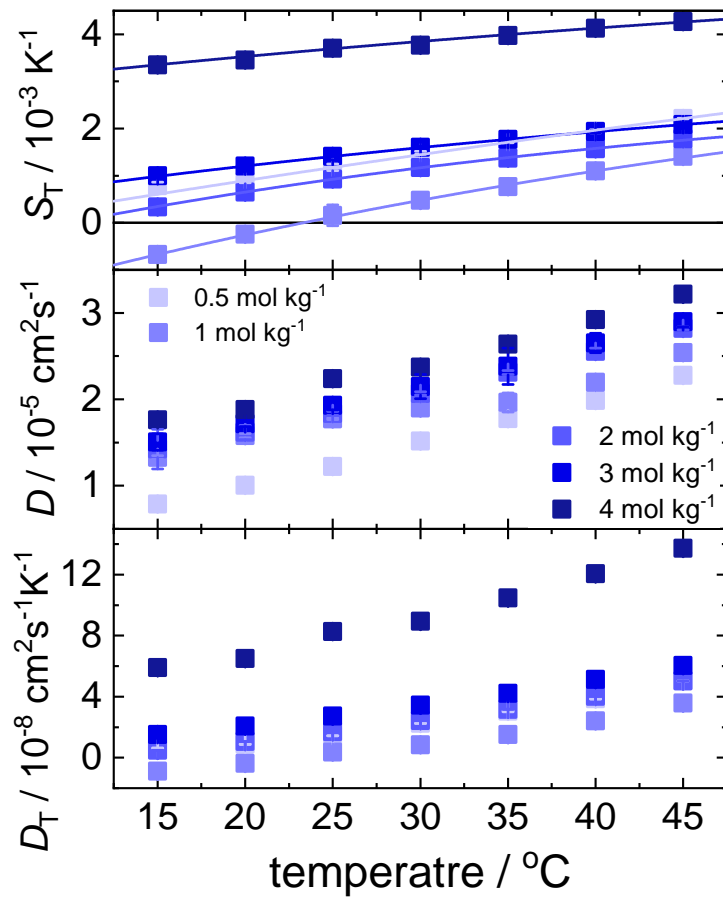


Figure S7: Temperature dependence of S_T, D_T and D of NaI at different concentrations as shown in inset. The darkest symbol corresponds to the highest concentration 4 mol/kg followed by lower concentrations of 3, 2, 1 and 0.5 mol/kg (faded symbol).

Table S2: The table enlists the fitting parameters obtained for NaI using Eq.2 in the main manuscript for all the concentrations studied

m / mol/kg	$S_T^\infty / 10^{-3} K^{-1}$	T^* / K	T^0 / K
0.5	10.32 ± 0.01	24.92 ± 2.16	52.7 ± 2.9
1	4.56 ± 0.12	23.31 ± 0.02	60.4 ± 2.3
2	3.20 ± 0.03	9.92 ± 0.52	44.1 ± 6.0
3	4.03 ± 0.02	-3.80 ± 0.50	67.0 ± 5.3
4	6.28 ± 0.01	-46.78 ± 10.28	81.00 ± 10.5

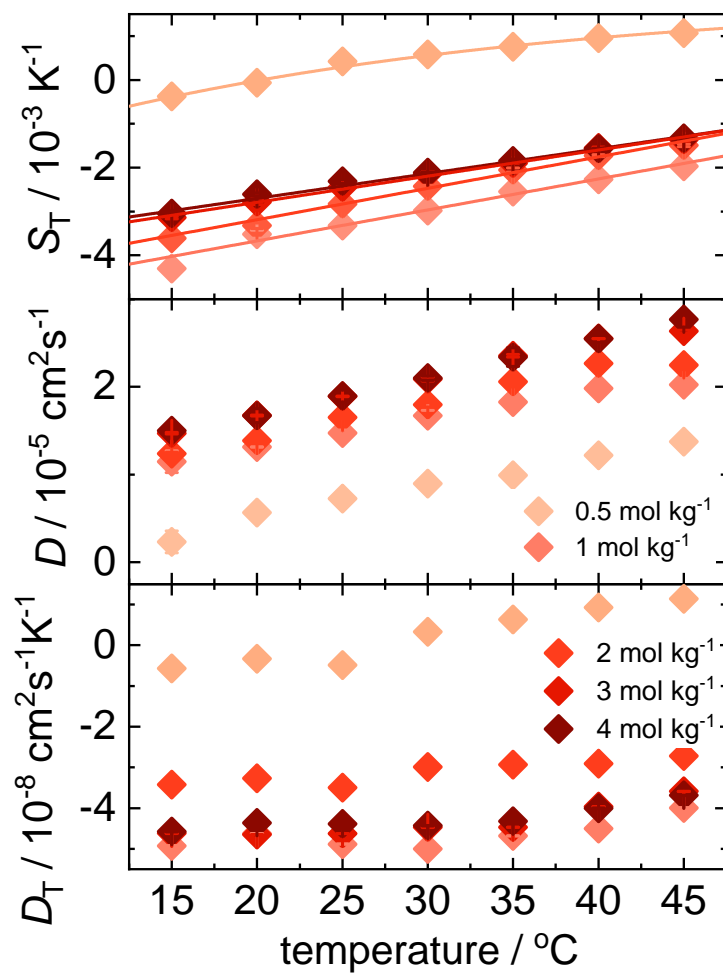


Figure S8: Temperature dependence of S_T , D_T and D of LiI at different concentrations as shown in inset. The darkest symbol corresponds to the highest concentration 4 mol/kg followed by lower concentrations of 3, 2, 1 and 0.5 mol/kg (faded symbol).

Table S3: The table enlists the fitting parameters obtained for LiI using Eq.2 in the main manuscript for all the concentrations studied

m / mol/kg	$S_T^\infty / 10^{-3} K^{-1}$	T^* / K	T^0 / K
0.5	1.91 ± 0.06	20.24 ± 0.49	28.2 ± 11.0
1	-2.58 ± 0.02	23.31 ± 0.02	23.1 ± 2.4
2	-2.39 ± 0.03	28.95 ± 0.089	32.6 ± 4.6
3	-3.59 ± 0.17	36.29 ± 0.59	46.9 ± 2.9
4	-8.95 ± 0.03	42.56 ± 1.03	48.5 ± 3.8

References

- [1] K. Thyagarajan and P. Lallemand. Determination of thermal-diffusion ratio in a binary mixture by forced rayleigh-scattering. *Opt. Commun.*, 26:54–57, 1978.
- [2] W. Köhler. Thermodiffusion in polymer-solutions as observed by forced rayleigh-scattering. *J. Chem. Phys.*, 98:660–668, 1993.
- [3] W. Köhler and P. Rossmanith. Aspects of thermal-diffusion forced rayleigh-scattering - heterodyne-detection, active phase tracking, and experimental constraints. *J. Phys. Chem.*, 99:5838–5847, 1995.
- [4] W. Köhler and R. Schäfer. Polymer analysis by thermal-diffusion forced rayleigh scattering. In *New Developments in Polymer Analytics II*, volume 151 of *Advances in Polymer Science*, pages 1–59. 2000.
- [5] S. Wiegand and W. Köhler. Measurement of transport coefficients by an optical grating technique. In Werner Köhler and Simone Wiegand, editors, *Thermal Nonequilibrium Phenomena in Fluid Mixtures*, volume 584, pages 189–210. Springer Berlin Heidelberg, Berlin, Heidelberg, 2002.
- [6] P. Blanco, H. Kriegs, M. P. Lettinga, P. Holmqvist, and S. Wiegand. Thermal diffusion of a stiff rod-like mutant y21m fd-virus. *Biomacromolecules*, 12:1602–1609, 2011.
- [7] S. Wiegand, H. Ning, and H. Kriegs. Thermal diffusion forced rayleigh scattering setup optimized for aqueous mixtures. *J. Phys. Chem. B*, 111:14169–14174, 2007.
- [8] G. Wittko and W. Köhler. Precise determination of the solet, thermal diffusion and mass diffusion coefficients of binary mixtures of dodecane, isobutylbenzene and 1,2,3,4-tetrahydronaphthalene by a holographic grating technique. *Philos. Mag.*, 83:1973–1987, 2003.
- [9] H. Ning, R. Kita, H. Kriegs, J. Luettmer-Strathmann, and S. Wiegand. Thermal diffusion behavior of nonionic surfactants in water. *J. Phys. Chem. B*, 110:10746–10756, 2006.
- [10] A. Becker, W. Köhler, and B. Müller. A scanning michelson interferometer for the measurement of the concentration and temperature derivative of the refractive- index of liquids. *Ber. Bunsen-Ges. Phys. Chem. Chem. Phys.*, 99:600–608, 1995.